Article

Cell Reports

Interrogation of Functional Cell-Surface Markers Identifies CD151 Dependency in High-Grade Serous Ovarian Cancer

Graphical Abstract

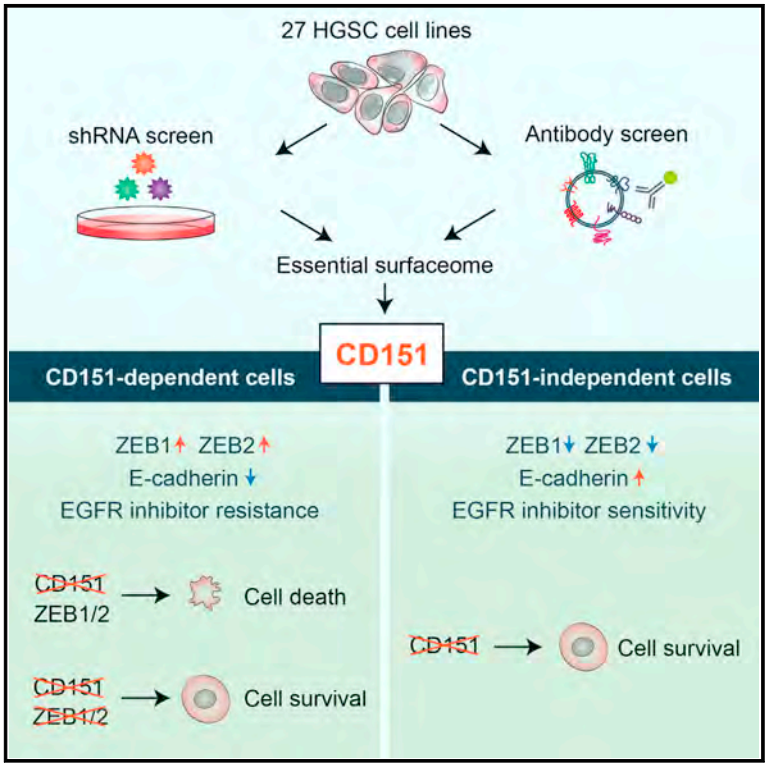

Highlights

- Pooled genome-wide RNAi screens and cell-surface analysis in HGSC cell lines
- A subset of HGSC lines is dependent on tetraspanin CD151 for survival
- CD151 supports tumor growth in vivo, and dependency is mediated by ZEB1 and ZEB2
- High CD151 expression is associated with poor prognosis in HGSC

Authors

Mauricio Medrano, Laudine Communal, Kevin R. Brown, ..., Laurie Ailles, Anne-Marie Mes-Massons, Robert Rottapel

Correspondence

rottapel@uhnresearch.ca

In Brief

Medrano et al. conduct whole-genome short hairpin RNA screens in 27 high-grade serous ovarian carcinoma (HGSC) cell lines to identify vulnerabilities in HGSC. Analysis of the cell surface reveals that CD151 is essential for cell survival through a ZEB-dependent mechanism.

Accession Numbers

GSE94304

Medrano et al., 2017, Cell Reports *18*, 2343–2358
March 7, 2017
http://dx.doi.org/10.1016/j.celrep.2017.02.028

CellPress

Cell Reports
Article

Interrogation of Functional Cell-Surface Markers Identifies CD151 Dependency in High-Grade Serous Ovarian Cancer

Mauricio Medrano,[1,2] Laudine Communal,[6,7] Kevin R. Brown,[9] Marcin Iwanicki,[10] Josee Normand,[1] Joshua Paterson,[1] Fabrice Sircoulomb,[1] Paul Krzyzanowski,[11] Marian Novak,[12] Sasha A. Doodnauth,[1,2] Fernando Suarez Saiz,[1] Jane Cullis,[14] Rima Al-awar,[11] Benjamin G. Neel,[1,15] John McPherson,[11] Ronny Drapkin,[13] Laurie Ailles,[1,2] Anne-Marie Mes-Massons,[6,7,8] and Robert Rottapel[1,2,3,4,5,16,*]

[1]Princess Margaret Cancer Center, University Health Network, Toronto, ON M5G 1L7, Canada
[2]Department of Medical Biophysics, University of Toronto, Toronto, ON M5G 1L7, Canada
[3]Department of Medicine, University of Toronto, Toronto, ON M5G 2C4, Canada
[4]Department of Immunology, University of Toronto, Toronto, ON M5S 1A8, Canada
[5]Division of Rheumatology, St. Michael's Hospital, Toronto, ON M5B 1W8, Canada
[6]Centre de Recherche du Centre Hospitalier de l'Université de Montréal (CRCHUM), Montreal, QC H2X 0A9, Canada
[7]Institut du Cancer de Montréal, Montréal, QC H2X 0A9, Canada
[8]Département de Médecine, Université de Montréal, Montreal, QC H3T 1J4, Canada
[9]Banting and Best Department of Medical Research, Donnelly Centre for Cellular and Biomolecular Research, University of Toronto, Toronto, ON M5S 3E1, Canada
[10]Department of Cell Biology, Harvard Medical School, Boston, MA 02115, USA
[11]Ontario Institute for Cancer Research, MaRS Centre, Toronto, ON M5G 1L7, Canada
[12]Department of Medical Oncology, Center for Molecular Oncologic Pathology, Dana-Farber Cancer Institute, Harvard Medical School, Boston, MA 02215, USA
[13]Ovarian Cancer Research Center, Department of Obstetrics and Gynecology, Perelman School of Medicine, University of Pennsylvania, Philadelphia, PA 19104, USA
[14]Department of Biochemistry and Molecular Pharmacology, New York University School of Medicine, New York, NY 10016, USA
[15]Laura and Isaac Perlmutter Cancer Centre, NYU Langone Medical Center, New York, NY 10016, USA
[16]Lead Contact
*Correspondence: rottapel@uhnresearch.ca
http://dx.doi.org/10.1016/j.celrep.2017.02.028

SUMMARY

The degree of genetic aberrations characteristic of high-grade serous ovarian cancer (HGSC) makes identification of the molecular features that drive tumor progression difficult. Here, we perform genome-wide RNAi screens and comprehensive expression analysis of cell-surface markers in a panel of HGSC cell lines to identify genes that are critical to their survival. We report that the tetraspanin CD151 contributes to survival of a subset of HGSC cell lines associated with a ZEB transcriptional program and supports the growth of HGSC tumors. Moreover, we show that high CD151 expression is prognostic of poor clinical outcome. This study reveals cell-surface vulnerabilities associated with HGSC, provides a framework for identifying therapeutic targets, and reports a role for CD151 in HGSC.

INTRODUCTION

Epithelial ovarian cancer (EOC) is the fifth leading cause of cancer-related deaths in women in North America and is responsible for over 100,000 deaths per year worldwide (Ferlay et al., 2015). High-grade serous carcinoma (HGSC) is the most common and lethal subtype, with the vast majority of women diagnosed at an advanced stage of disease (Bast et al., 2009). The current standard treatment is surgical debulking combined with adjuvant and/or neo-adjuvant platinum and taxane-based chemotherapy. While standard therapy induces an initial response, tumors ultimately recur, and 70% of patients die within 5 years of diagnosis (Bast et al., 2009). Developing a deeper understanding of the molecular and cellular features that drive HGSC progression may, therefore, allow for the identification of better therapeutic targets and ultimately improve the prognosis of women with HGSC.

The development of targeted therapies for human cancers has been guided by the discovery of cancer-specific genetic aberrations including gene fusions, gain-of-function mutations, and gene amplifications that contribute to the pathogenesis of different tumor types (Weinstein, 2002). While this strategy has led to the approval of several promising therapies, many tumor types exhibit a high degree of genetic abnormalities with no single discernable oncogenic driver. Moreover, many established oncogenic drivers remain undruggable, such as mutant RAS and MYC. HGSC features a damaged genome, characterized by widespread gene amplifications, deletions, and chromosomal fragmentation, with a paucity of dominantly acting oncogenes.

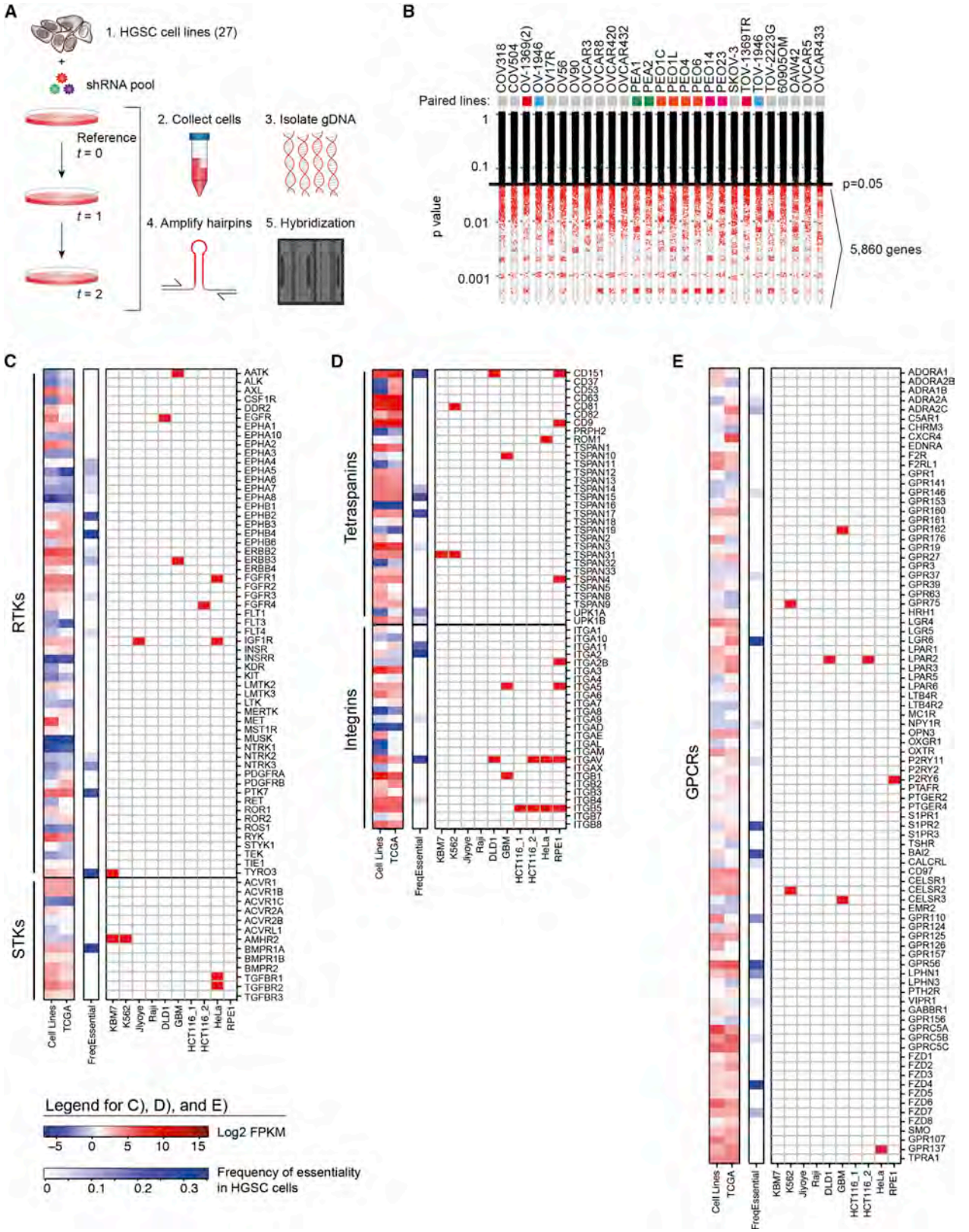

(legend on next page)

The single unifying genetic feature of HGSC is the near-ubiquitous mutation of *TP53*. Inactivating mutations in *BRCA1* and *BRCA2*, observed in 17% and 3% of germline and somatic cases, respectively, are the next most common mutations (Cancer Genome Atlas Research Network, 2011). Therapies targeting vascular endothelial growth factor (VEGF) (bevacizumab) and poly(ADP-ribose) polymerase (PARP) (olaparib) in HGSC have shown variable efficacy in a subset of patients (Burger et al., 2011; Ratner et al., 2012). Therefore, there is a continued need to identify therapeutic targets for HGSC. Transcriptional profiling of HGSC tumors uncovered four transcriptional subtypes (differentiated, immunoreactive, mesenchymal, and proliferative) that may exhibit distinct molecular dependencies and could potentially respond to subtype-directed therapies (Cancer Genome Atlas Research Network, 2011).

Genome-wide RNAi screens have revealed synthetic lethal associations between gene targets and genetic abnormalities in cancer cells that can be exploited to impair the survival of tumor cells (Barbie et al., 2009; Luo et al., 2008; Moffat et al., 2006). Integration of functional genomic approaches with gene expression and copy number studies can reveal unanticipated gene dependencies associated with specific molecular features (Kim et al., 2013; Marcotte et al., 2012, 2016). Genes encoding cell-surface proteins that support tumor growth are attractive targets, because they are highly amenable to therapeutic antibodies. Moreover, antibody-directed therapies can be used to deliver toxic payloads in the form of antibody-drug conjugates (Gerber et al., 2013). We performed a comprehensive genomic analysis and functional characterization of a large collection of HGSC cell lines to map the surface molecular vulnerabilities associated with HGSC.

RESULTS

Functional Surfaceome of HGSC

To identify cell lines representative of the molecular features of HGSC, we assessed gene copy number aberration (CNA) and nonsynonymous somatic variants in a panel of 40 EOC cell lines: 32 HGSC, 6 clear cell, and 2 of unknown histotype (Table S1). Twenty-two of 32 HGSC cell lines were derived from individual patients, and the remaining 10 were isogenic pairs of one of the 22 cell lines. We used a previously published scoring methodology to identify cell lines with common features of HGSC (Domcke et al., 2013). The score rewards cell lines with mutant *TP53* and strong correlation between the cell line CNA profile and the mean CNA profile of TCGA (The Cancer Genome Atlas) tumors, and it penalizes cell lines with a hypermutator phenotype (more than ten mutations per million bases) and with mutations in genes associated with non-HGSC subtypes (*PIK3CA*, *PTEN*, *ERBB2*, *KRAS*, *BRAF*, *CTNNB1*, and *ARID1A*). Thirty-two of our cell lines contained *TP53* mutations, 17 of which did not contain mutations in genes associated with other EOC subtypes (Figure S1A; Table S1). Thirteen lines in our panel were previously evaluated, and comparison of published and independently calculated suitability scores revealed a strong correlation (Figure S1B). Together, these data indicate that HGSC cell lines are representative of the major genetic events associated with HGSC biology and reinforce their utility as in vitro surrogate models of HGSC.

To identify genes that support the survival of HGSC cell lines, we performed genome-wide functional genetic screens on 27 HGSC cell lines (Figure 1A). We stably transduced cell lines with a library of 78,432 hairpins targeting 16,052 genes in a pooled format and monitored for genes that, when depleted, impaired the relative fitness of each cell line (Moffat et al., 2006). Cell lines were screened in triplicate, and overall short hairpin (sh) RNA (shRNA) abundance was assessed during population outgrowth for multiple time points. shRNA Activity Ranking Profile (shARP) scores were assigned to hairpins by calculating the average slope between the microarray intensity of shRNA probes at each time point and time 0. To evaluate the behavior of specific genes, the normalized Gene Activity Ranking Profile (zGARP) score was calculated as the average of the two lowest shARP scores (Marcotte et al., 2012). We identified 5,860 candidate genes with significant zGARP scores (Figure 1B), and genes that scored in greater than 50% of cell lines (278 genes) populated components of the spliceosome, ribosome, proteasome, DNA replication, protein metabolism/transport, and mRNA processing.

Genes encoding integral membrane proteins and cell-surface receptors were prioritized as potential therapeutic targets. We summarized median gene expression across 27 HGSC cell lines and compared it to the average expression in 404 HGSC tumors from the TCGA dataset. The expression data were aligned with the frequency of essentiality and categorized in gene clusters, including a kinase cluster of 57 receptor tyrosine kinases and 13 serine/threonine kinases (Figure 1C), a cell-adhesion cluster of 31 tetraspanins and 25 integrins (Figure 1D), and 86 G-protein-coupled receptors (GPCRs) (Figure 1E). All other surface protein-encoding genes are represented in Figure S1C. We used a CRISPR (clustered regularly interspaced short palindromic repeat)-screen dataset from ten cell lines of various tissue types to identify HGSC-specific essential genes (Hart et al., 2015). Inspection of genes with a high frequency of essentiality, as well as high expression in HGSC cell lines and tumors, confirmed known proto-oncogenic targets in ovarian cancer, including *ERBB3*, *EPHB4*, and *BMPR1A*, which contribute to cell survival and chemotherapeutic resistance (Hover et al., 2015; Kumar et al., 2007; Sheng et al., 2010). Our integrated

Figure 1. Functional Surfaceome of HGSC

(A) Schematic of shRNA screens. gDNA, genomic DNA.

(B) RNAi screen summary for 27 HGSC cell lines. Candidate genes with normalized Gene Activity Ranking Profile (zGARP) scores with $p < 0.05$ are highlighted in red (n = 5,860).

(C–E) Expression and essentiality of (C) receptor tyrosine kinases (RTKs) and serine/threonine kinases (STKs), (D) tetraspanins and integrins, and (E) G-protein-coupled receptors (GPCRs) in HGSC cell lines and TCGA tumors. Non-HGSC cell lines from a CRISPR-screen dataset (Hart et al., 2015) are shown on the right, and genes identified as essential are indicated in red. FPKM, fragments of kilobase of exon per million fragments mapped.

See also Figure S1 and Table S1.

functional genomic approach revealed potential cell-surface targets, including kinases *PTK7* and *TYRO3*; tetraspanins *CD151*, *TSPAN14*, *TSPAN15*, and *TSPAN17*; and GPCRs *LGR6*, *S1PR2*, *BAI2*, *GPR110*, *GPR56*, and *FZD4*.

Cell-Surface Characterization of HGSC

To characterize the expression of surface targets, we examined protein expression in 26 HGSC cell lines and 3 cell lines derived from normal fallopian tube epithelium (FTE), the most common cellular origin of HGSC. Cell lines were profiled by high-throughput flow cytometry using 371 fluorochrome-conjugated cell-surface antibodies (Figures 2A and S2A; Data File S1), targeting cell-adhesion molecules, immune receptors, cytokine receptors, differentiation markers, and receptor protein kinases (Gedye et al., 2014). Independent screens using TOV-1369TR and OV-1369(2) cells demonstrated strong correlations of 0.85 and 0.90, respectively (Figures S2B and S2C), indicating that the platform can reproducibly identify similar proportions of antigen-positive cells.

Across the cell-line panel, 214 of 371 (58%) antibodies stained negative or marked a subpopulation of cells (<50% positive cell populations) (Figure S2D). Of the remaining 157 markers, 83 were present in less than 30% of cell lines. Only 13 markers were detected on the surface across all cell lines (Figure S2D). Analysis of cell-surface marker profiles of HGSC and FTE cells revealed 30 antigens overexpressed in FTE cells and, notably, several tumor necrosis factor family ligands and receptors (Figure 2B). Targets with relatively low expression in HGSC cells included CD82, DPP4, and THY1, which are downregulated or associated with tumor suppression in ovarian cancer (Abeysinghe et al., 2003; Kajiyama et al., 2003; Liu et al., 2000). Only CDCP1 and FZD4 were identified at higher levels in HGSC cells relative to FTE cells.

Intersection of the RNAi and antibody-screen datasets identified previously known and unknown candidate targets in HGSC (Figure 2C). We prioritized targets that were present in a greater-than-50%-positive population in each cell line and were discovered as a hit by RNAi in more than 10% of cell lines. Inspection of hairpin dropout profiles revealed 11 candidates with consistent hairpin activities that were selected for further validation (Figure 2D). We tested the top two scoring hairpins against each target from the original RNAi screen and noted pronounced toxicity in cell lines expressing hairpins targeting the tetraspanin *CD151* (Figure 2D). High expression of *CD151* has been previously associated with poor prognosis in several human cancers (Haeuw et al., 2011). Moreover, interrogation of *CD151* dependency in ovarian, breast, and pancreatic cancer cell lines from our published dataset (Marcotte et al., 2012, 2016) identified *CD151* as a potential functional target in other epithelial cancers (Figure 2E). Based on the high expression of *CD151* in HGSC cell lines and TCGA tumors, the frequency of essentiality of *CD151* in the shRNA dropout screens, and its high cell-surface expression within HGSC cell lines, we decided to investigate the role of *CD151* in HGSC in more detail.

CD151 Is Required for Survival and Mesothelial Cell Clearance in a Subset of HGSC Cell Lines

To thoroughly examine CD151 dependency, we stably depleted CD151 with two hairpins in 15 HGSC cell lines and observed a 50%–90% decrease in viability in 6 of 15 cell lines, suggesting that CD151 is important for viability in a subset of cell lines (Figure S3A). To verify that the decrease in cell viability was not an artifact of shRNA-mediated knockdown, we transiently transfected cell lines with a pool of siRNAs targeting *CD151* and found a significant correlation in survival profiles with shRNA depletion (Figures S3B and S3C). In a more extensive interrogation, depletion of CD151 using four distinct hairpins significantly impaired proliferation of TOV-1946 and OVCAR8 cells, while PEA1 and OVCAR433 cells showed minimal differences in proliferation relative to shGFP-expressing cells (Figure 3A). Depletion of CD151 has been reported to increase proliferation of ovarian cancer cell lines OVCAR5 and OVCAR420 (Baldwin et al., 2014); however, we observed that these cells did not demonstrate an increase in their proliferative capacity after CD151 knockdown (Figures S3D and S3E). Ablation of CD151 induced cell death in TOV-1946 and OVCAR8 cells (Figure 3B) and impaired colony formation in OVCAR8 cells (Figure S3F). To confirm the causal role of CD151 in HGSC cell survival, we overexpressed shRNA-resistant *CD151* cDNA in OVCAR8 cells and rescued the death phenotype (Figures S3G–S3I). Interestingly, following long-term growth of CD151-depleted cells, we observed that CD151 was re-expressed in one of eight and in three of seven long-term growth populations of OVCAR8 and TOV-1946 cells, respectively, indicating a selective pressure for maintaining CD151 expression (Figures S3J and S3K).

CD151 interacts with laminin-binding integrins and can promote activation of downstream integrin effectors, including focal adhesion kinase (FAK) and SRC (Hemler, 2005). Depletion of CD151 decreased activation of FAK and SRC in CD151-dependent OVCAR8 cells compared with control hairpin-expressing cells (Figure 3C). Collectively, these data suggest that a subset of HGSC cell lines is exquisitely sensitive to CD151 knockdown.

We next examined the requirement for CD151 in three-dimensional cell growth. Stable depletion of CD151 impaired spheroid formation compared to cells expressing shGFP (Figures 3D and 3E). Comparison of ethidium bromide (EtBr) uptake in cellular clusters depleted of CD151 compared with shGFP-expressing clusters demonstrated increased uptake in OVCAR8 clusters 24–48 hr following stable knockdown of CD151 (Figure 3F). In contrast, no change in EtBr uptake was observed in PEA1 clusters depleted of CD151 relative to shGFP-expressing cells (Figure 3F). Dissemination of HGSC involves the implantation of spheroids into the mesothelial layer lining peritoneal organs (Burleson et al., 2004). We examined the interaction between OVCAR8 and PEA1 spheroids and mesothelial cells using live in vitro imaging (Iwanicki et al., 2011) and found that depletion of CD151 significantly impaired invasion of the mesothelial layer by OVCAR8 cells, whereas PEA1 cells demonstrated no change in mesothelial clearance (Figure 3G; Movies S1 and S2). These data indicate that CD151 is differentially required for anchorage-independent viability of HGSC cells and for implantation into a mesothelial layer in vitro.

CD151 Supports HGSC Xenograft Initiation and Maintenance

To determine the contribution of CD151 to tumor initiation in vivo, OVCAR8 and TOV-1946 cells stably expressing hairpins

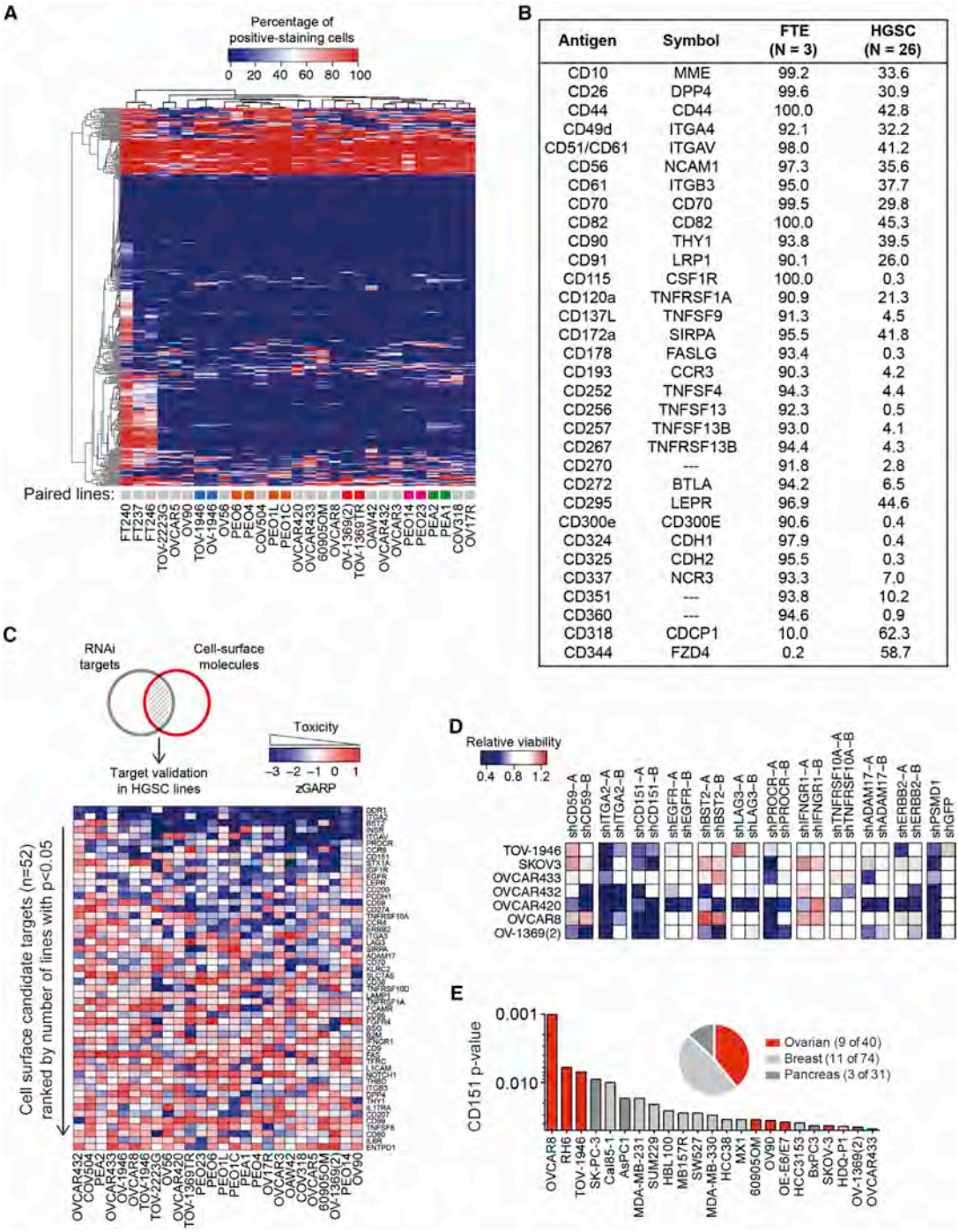

Antigen	Symbol	FTE (N = 3)	HGSC (N = 26)
CD10	MME	99.2	33.6
CD26	DPP4	99.6	30.9
CD44	CD44	100.0	42.8
CD49d	ITGA4	92.1	32.2
CD51/CD61	ITGAV	98.0	41.2
CD56	NCAM1	97.3	35.6
CD61	ITGB3	95.0	37.7
CD70	CD70	99.5	29.8
CD82	CD82	100.0	45.3
CD90	THY1	93.8	39.5
CD91	LRP1	90.1	26.0
CD115	CSF1R	100.0	0.3
CD120a	TNFRSF1A	90.9	21.3
CD137L	TNFSF9	91.3	4.5
CD172a	SIRPA	95.5	41.8
CD178	FASLG	93.4	0.3
CD193	CCR3	90.3	4.2
CD252	TNFSF4	94.3	4.4
CD256	TNFSF13	92.3	0.5
CD257	TNFSF13B	93.0	4.1
CD267	TNFRSF13B	94.4	4.3
CD270	---	91.8	2.8
CD272	BTLA	94.2	6.5
CD295	LEPR	96.9	44.6
CD300e	CD300E	90.6	0.4
CD324	CDH1	97.9	0.4
CD325	CDH2	95.5	0.3
CD337	NCR3	93.3	7.0
CD351	---	93.8	10.2
CD360	---	94.6	0.9
CD318	CDCP1	10.0	62.3
CD344	FZD4	0.2	58.7

Figure 2. Cell-Surface Characterization of HGSC

(A) Clustering of HGSC cell lines by percent positive cells (Data File S1).

(B) Percent positive cells for cell-surface antigens with a greater-than-50% difference expression between FTE and HGSC cells.

(C) Representation of zGARP scores for antigens detected by antibody screening and identified as essential by RNAi.

(D) Cell viability of HGSC cell lines expressing shRNA targeting the indicated genes. shRNAs targeting PSMD1 and GFP were used as positive and negative controls, respectively.

(E) Representation of 23 cell lines with significant zGARP scores ($p < 0.05$) and ranked by p value from screens of 145 cell lines of ovarian, breast, and pancreas tumors. The fraction of cell lines from each tumor type is depicted by the pie chart.

See also Figure S2 and Data File S1.

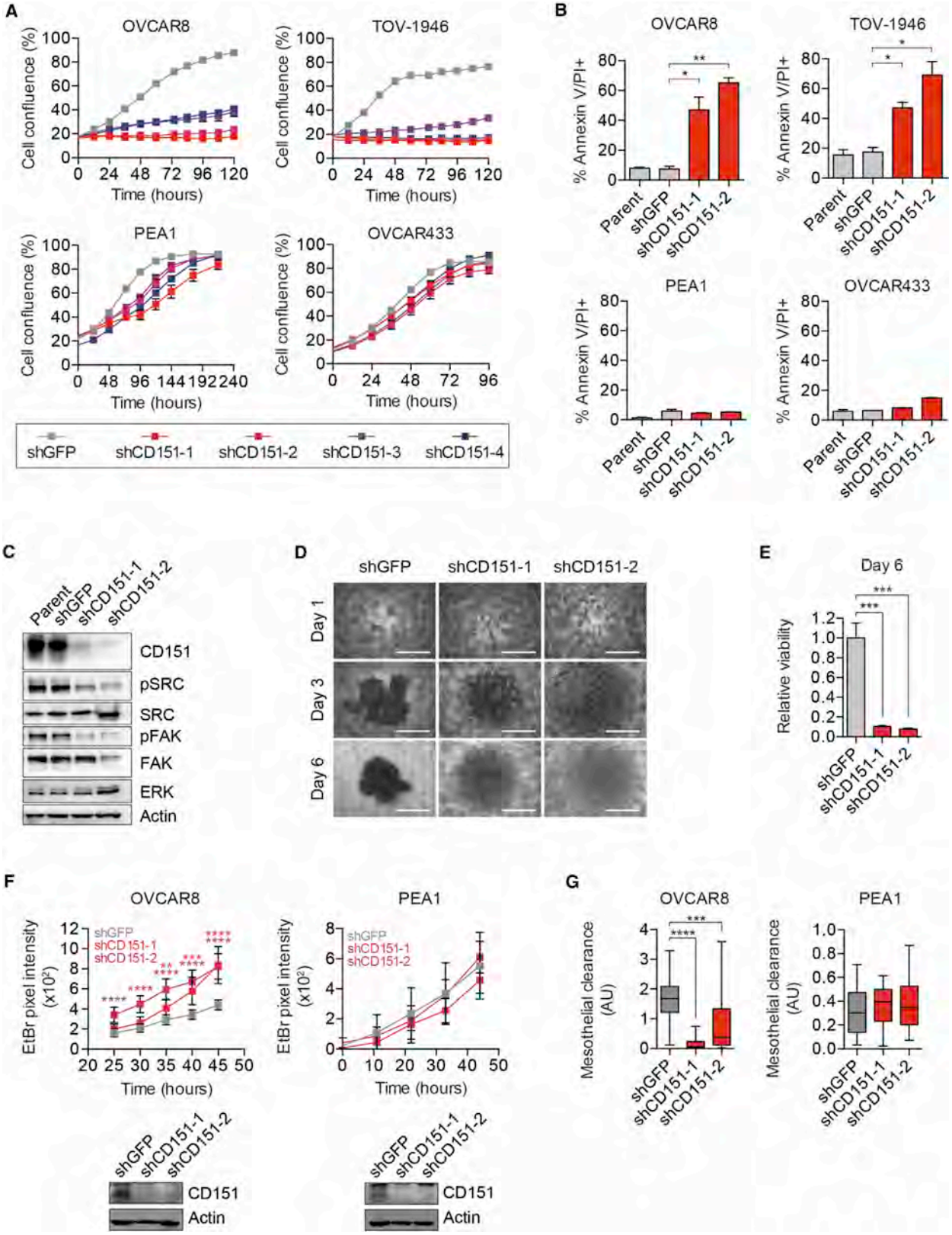

(legend on next page)

targeting *CD151* or control shGFP were injected into the mammary fat pad of immunodeficient NOD/SCID/IL2R$\gamma^{-/-}$ (NSG) mice. CD151-depleted xenografts exhibited 62%–90% and 74%–89% attenuation in tumor growth relative to shGFP-expressing cells in OVCAR8 and TOV-1946 cells, respectively (Figures 4A, 4B, S4A, and S4B). To ascertain the role of CD151 in the maintenance of tumor growth, doxycycline (dox)-inducible shRNAs were stably introduced into OVCAR8 cells. Treatment of OVCAR8 cells in vitro with 1 μg/mL dox resulted in the depletion of CD151 by 24 hr, accompanied by a severe impairment of cell proliferation (Figures S4C and S4D). OVCAR8 cells expressing dox-inducible shRNA were implanted into the mammary fat pad, and mice were treated with 5% sucrose (vehicle control), 5% sucrose and dox from onset (Dox D0), or 5% sucrose and dox at 21 days post-implantation (Dox D21) (Figure S4E). Consistent with our stable knockdown studies, mice in the Dox D0 group demonstrated a 70% reduction in the growth of tumors expressing hairpin targeting CD151 relative to shGFP-expressing tumors and the vehicle control group (Figures 4C, 4D, and S4F). Tumors in the Dox D21 group were 82% smaller than tumors in the vehicle control group and 74% smaller than shGFP-expressing tumors (Figures 4E and S4F). Importantly, these data were recapitulated in an intraperitoneal xenograft model of ovarian cancer to emulate the clinical behavior of this disease (Figures 4F, 4G, and S4G–S4I). Together, these data show that CD151 is required for tumor initiation and maintenance in HGSC xenograft models.

CD151 Dependency Is Coupled to a ZEB1 and ZEB2 Transcription Factor Network

We next sought to investigate the molecular features that distinguish CD151-dependent and CD151-independent cell lines. We hypothesized that differences in CD151 expression could account for differential CD151 dependency. CD151 RNA and protein expression varied by 8- and 10-fold, respectively, and were significantly correlated across HGSC cell lines (Figure S5A). However, we found poor correlation of expression of CD151 with sensitivity to CD151 depletion (Figure S5B). Analysis of CD151 localization did not reveal differences between CD151-dependent and CD151-independent cells (data not shown).

Integrins $\alpha_6\beta_1$, $\alpha_3\beta_1$, and $\alpha_6\beta_4$ interact with CD151 and can have pro-tumor functions (Desgrosellier and Cheresh, 2010). We examined whether these integrins were differentially expressed in CD151-dependent versus -independent cell lines and observed that integrin surface expression levels did not correspond with CD151 dependency (Figure S5C). CD151 can exist on the cell surface in integrin-associated and integrin-free forms, which can be distinguished by monoclonal antibodies (mAbs) that recognize total cell-surface CD151 (11G5a) and integrin-free CD151 (mAb 1A5) (Palmer et al., 2014). Analysis of CD151 expression in 13 HGSC cell lines using mAbs 11G5a and 1A5 uncovered a positive correlation between the proportion of integrin-free CD151 and CD151 dependency (Figure S5D). Further, by co-precipitation experiments, we found that CD151:β_1 and CD151:β_4 complexes were enriched in CD151-independent cell lines (Figures S5E and S5F). These data suggest that CD151 dependency can be attributed to a non-integrin-mediated mechanism.

To identify genes associated with CD151 dependency, we examined gene expression by RNA sequencing (RNA-seq) and found 789 transcripts differentially expressed between CD151-dependent versus -independent cell lines (Figure 5A; Data File S2). We noted that several genes associated with epithelial-to-mesenchymal transition (EMT) (*ZEB1*, *ZEB2*, *CXCR2*, and *DNAJC6*) were enriched in CD151-dependent cells, whereas epithelial-specific genes (*CDH1*, *CLDN4*, *EPCAM*, *FOXA2*, and *OVOL1*) were enriched in CD151-independent cells (Brabletz and Brabletz, 2010; Kohn et al., 2014; Song et al., 2010; Yang et al., 2014; Zhou et al., 2015); differential protein expression was verified for several transcripts (Figure 5B). Gene set enrichment analysis (GSEA) of transcript profiles revealed genes upregulated in mammary stem cells, invasive breast cancer, and targets of transforming growth factor beta 1 (TGF-β1) as significantly associated with CD151 dependency (Figure S5G; Table S2). Genes expressed at higher levels in CD151-independent cells were enriched for epithelial-specific genes repressed by ZEB1, downregulated during TGF-β1-induced EMT, and associated with sensitivity to gefitinib (Figures 5C and S5H; Table S2).

ZEB1 (*TCF8*/*δEF1*) and *ZEB2* (*SIP1*), which are transcription factors that promote EMT by repressing various epithelial genes, were upregulated in CD151-dependent cells, whereas high expression of other known master regulators of EMT (*SNAI1*, *SNAI2*, and *TWIST1*) was not observed. A critical role for *ZEB1* and *ZEB2* was further supported by the increased expression of genes downstream of TGF-β and RB1, regulators of *ZEB1* and *ZEB2*, in CD151-dependent cells (Table S2), and an enrichment of *ZEB1* targets in CD151-independent cells (Aigner et al., 2007; Arima et al., 2012; Zavadil and Böttinger, 2005) (Figure S5H; Table S2).

Figure 3. CD151 Is Required for Survival and Mesothelial Cell Clearance in a Subset of HGSC Cell Lines

(A) Growth curves of cell lines expressing shGFP or shCD151. Error bars indicate mean ± SEM; n = 4.

(B) Quantification of annexin V and propidium iodide (PI) staining in cell lines expressing shGFP or shCD151. Error bars indicate mean ± SEM. *p < 0.05; **p < 0.01.

(C) Immunoblot analysis of phosphorylated SRC (pSRC) and phosphorylated FAK (pFAK) in CD151-depleted OVCAR8 cells and in shGFP-expressing cells. ERK and actin serve as protein loading controls.

(D) Phase-contrast images of OVCAR8 spheroids in a hanging drop expressing shGFP or shCD151. Scale bars represent 100 μm.

(E) Quantification of the viability of spheroids shown in (D). Error bars indicate mean ± SEM. ***p < 0.001.

(F) Ethidium bromide (EtBr) pixel intensity within the cluster area quantified over time in OVCAR8 and PEA1 cellular clusters cultured under detached conditions. CD151 protein levels were assessed by immunoblot, and actin serves as a protein loading control. For OVCAR8 cellular clusters, values represent the mean of shGFP (n = 9)-, shCD151-1 (n = 8)-, and shCD151-2 (n = 9)-expressing cells. For PEA1 cellular clusters, five clusters were analyzed per condition. Data are representative of two independent experiments. Error bars indicate mean ± SEM. **p < 0.01; ***p < 0.001; ****p < 0.0001.

(G) Quantification of mesothelial cell clearance by OVCAR8 and PEA1 cell clusters expressing control shGFP or shCD151. Data are representative of two independent experiments; n = 10 per condition; boxplot whiskers extend to maximum and minimum values. ***p < 0.001; ****p < 0.0001.

See also Figure S3 and Movies S1 and S2.

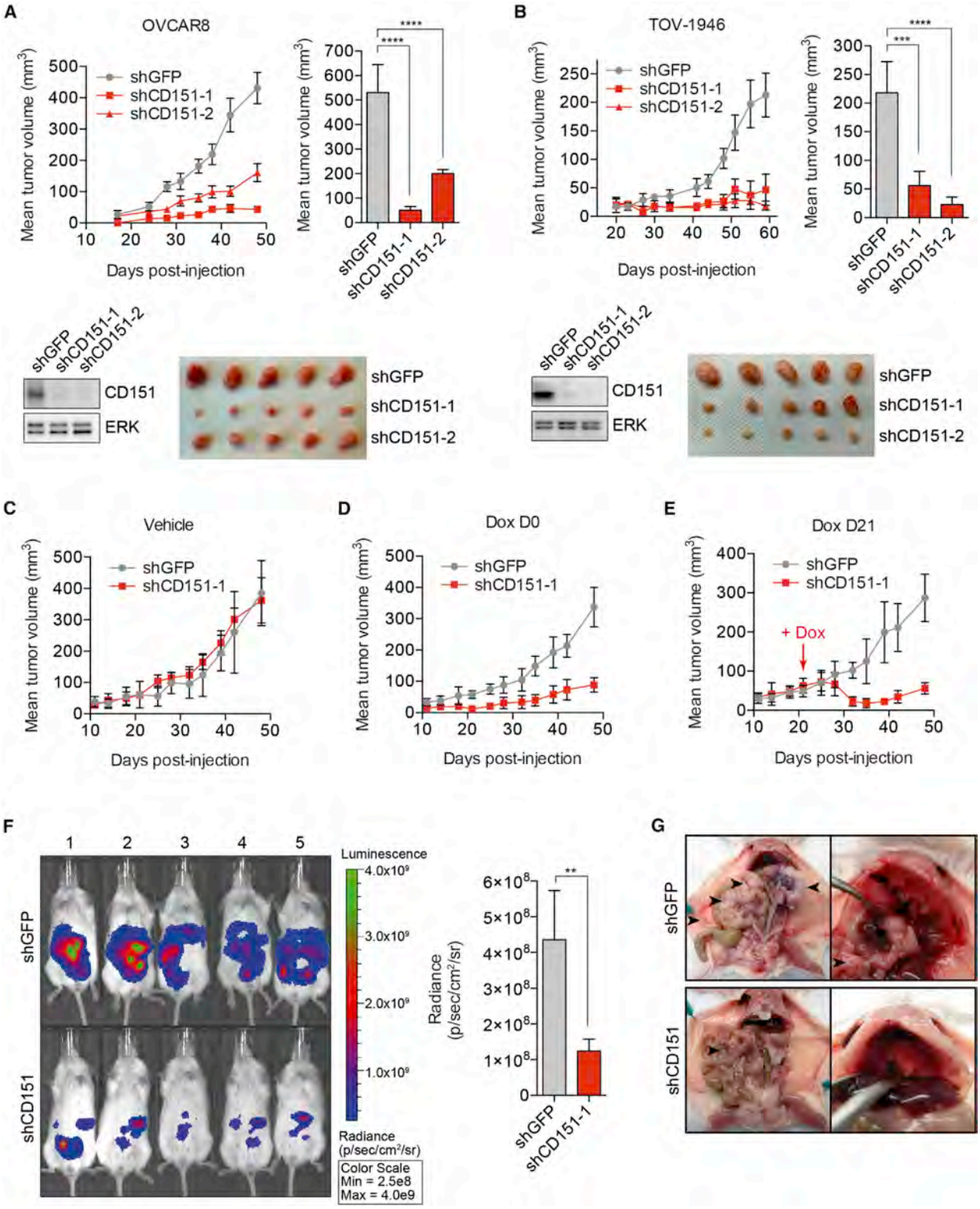

(legend on next page)

To identify chemical perturbations that track with CD151 dependency, we treated HGSC cell lines with a library of 400 small molecule kinase inhibitors and identified 25 compounds with toxicity profiles that discriminated between dependent and independent lines (Figure 5D). Notably, 11 of 25 compounds annotated as epidermal growth factor receptor (EGFR) inhibitors displayed increased toxicity in CD151-independent cells. Consistent with our findings in HGSC cell lines, non-small-cell lung cancer (NSCLC) cells that express low levels of ZEB1 and ZEB2 are sensitive to EGFR inhibition (Byers et al., 2013; Shien et al., 2013). Conversely, NSCLC cells that manifest a mesenchymal phenotype through increased expression of ZEB1 and ZEB2 are resistant to EGFR inhibitors (Byers et al., 2013; Shien et al., 2013). Dose response in CD151-dependent and CD151-independent cells demonstrated a 70-fold increase and a 270-fold increase in GI_{50} (50% of maximal inhibition of cell proliferation) values for erlotinib and gefitinib activity, respectively (Figures 5E and 5F). Taken together, these data suggest that CD151 dependency is linked to a ZEB1/ZEB2 network and corresponds with EGFR inhibitor resistance.

ZEB1 and ZEB2 Mediate Sensitivity to CD151 Suppression

Given that both ZEB1 and ZEB2 were highly elevated in CD151-dependent cells, we examined whether depletion of these genes was sufficient to revert the CD151-dependent phenotype. We stably infected CD151-dependent OVCAR8 and TOV-1946 cells with hairpins targeting *ZEB1* or *ZEB2* and observed no difference in proliferation compared with shGFP-expressing cells (Figures 6A, 6B and S6A–S6C). Depletion of CD151 alone resulted in impaired proliferation, which was restored when ZEB1 or ZEB2 were co-depleted (Figures 6A, 6B, and S6A–S6C). Consistent with these data, depletion of CD151 and ZEB2 prevented cell death, as determined by annexin V and propidium iodide (PI) staining (Figures 6C, S6D, and S6E). Moreover, depletion of ZEB1 or ZEB2 in CD151 knockdown cells restored FAK and SRC phosphorylation, compared to that in shGFP-expressing cells (Figure 6D). Together, these data show that ZEB1 and ZEB2 mediate CD151-dependent signaling and survival in HGSC cell lines.

The CD151-Dependent Phenotype Resembles the Mesenchymal Subtype of HGSC, and High CD151 Expression Is Associated with Poor Prognosis

HGSC can be subdivided into differentiated, mesenchymal, proliferative, and immunoreactive transcriptional subtypes (Cancer Genome Atlas Research Network, 2011), and patients in the mesenchymal subgroup have the worst outcome (Verhaak et al., 2013). We compared the gene set used to describe the TCGA subtypes to the CD151 dependency signature and found 15, 15, 5, and 21 common genes in the mesenchymal, proliferative, immunoreactive, and differentiated subtypes, respectively (Figure 7A). The expression profile of the mesenchymal, proliferative, immunoreactive, and differentiated subtypes matched that of CD151 dependence for 14 of 15 (93%), 8 of 15 (53%), 1 of 5 (20%), and 0 of 21 (0%) genes, respectively, suggesting that CD151-dependent cells most resemble the mesenchymal subtype. When the CD151 dependency signature was compared with the mesenchymal/de-differentiated HGSC signature from an independent dataset (Tothill et al., 2008), 7 of 11 and 30 of 45 genes were mutually upregulated and downregulated, respectively (Table S3).

Using immunofluorescence staining, we next evaluated CD151 expression and protein localization in serous tubal intraepithelial carcinoma (STIC) precursor lesions (defined by p53-positive staining and morphology), compared with regions of normal FTE. In normal polarized FTE, CD151 was constrained to the basolateral membrane, whereas in the STIC lesions, CD151 was detected uniformly on the cell membrane (Figure 7B). CD151 was overexpressed in one STIC lesion (case 1551_D15), compared with the adjacent normal epithelium (Figure 7B), and detected in detached HGSC cells proximal to the STIC (Figure S7A). High expression of CD151 was also observed in both the STIC and its contiguous invasive carcinoma (Figure S7B). Similarly, CD151 exhibited non-polarized membrane localization in HGSC tissue (Figure 7C). These data show that CD151 distribution and expression levels are altered, both in STIC lesions and in advanced HGSC.

To determine whether CD151 expression was associated with patient outcome in HGSC tumors, we evaluated CD151 protein levels by immunofluorescence in 500 primary human HGSC tumors from the Canadian Ovarian Experimental Unified Resource (COEUR) cohort (Figures 7D and S7C). Segregation of patients by high- and low-CD151 mean fluorescence intensity revealed reduced overall survival (OS) in patients with high expression of CD151, with a median OS of 37 months versus 55 months, and significantly reduced disease-free survival (DFS), with a median DFS of 12 months versus 19 months (Figure 7D). In a cohort of 82 primary human tumors, we found a significant difference in OS and DFS between $CD151^{hi}$ and $CD151^{lo}$ tumors and between $ZEB2^{hi}$ and $ZEB2^{lo}$ tumors (Figures S7C and S7D), which was

Figure 4. CD151 Supports HGSC Xenograft Initiation and Maintenance

(A and B) Growth curves and final tumor volume of (A) OVCAR8 and (B) TOV-1946 xenografts expressing shGFP or shRNA targeting CD151, represented as mean tumor volume. CD151 protein levels were assessed by immunoblot, and ERK serves as a protein loading control. Error bars indicate mean ± SEM; n = 5. ***p < 0.001; ****p < 0.0001. Images of dissected xenografts are shown.

(C–E) Growth curves of OVCAR8 xenografts expressing doxycycline (Dox)-inducible control shGFP or shCD151 represented as mean tumor volume. Mice were treated with (C) vehicle (5% sucrose); (D) doxycycline beginning on the day of injection (D0) (5% sucrose + 1 mg/mL dox in drinking water ad libitum); or (E) doxycycline 21 days after injection (D21). Error bars indicate mean ± SEM; n = 5.

(F) Representative images of in vivo expression of the luciferase reporter gene in OVCAR8 intraperitoneal xenografts expressing control shGFP or shCD151 at 46 days (left) and quantification of luminescence (right) expressed as radiance (photons/second/square centimeter/steradian; p/sec/cm^2/sr). Error bars indicate ± SEM; n = 5; **p < 0.005.

(G) Representative images of gross anatomy (left) and diaphragm (right) of tumor lesions of OVCAR8 xenografts expressing shGFP or shCD151. Arrowheads denote tumor tissue.

See also Figure S4.

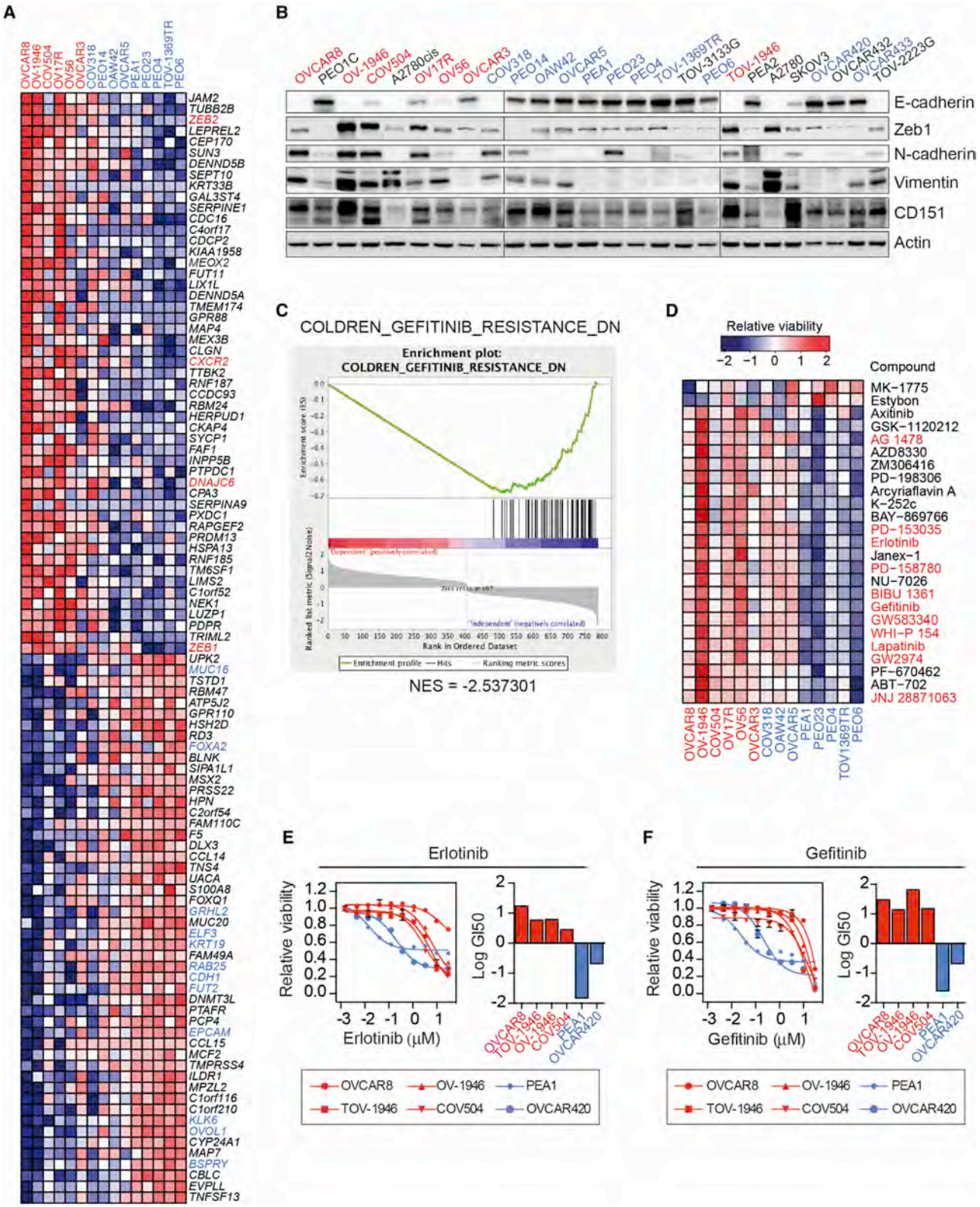

(legend on next page)

more significant when we compared CD151^{hi}/ZEB2^{hi} with CD151^{lo}/ZEB2^{lo} tumors (Figures 7E). Collectively, these data suggest that CD151 may promote and/or support progression of HGSC tumors and that high CD151 and ZEB2 expression in primary human disease is predictive of poor outcome.

DISCUSSION

Modulation of CD151 levels by RNAi or overexpression, or treatment with mAbs targeting CD151, has demonstrated a convincing role for CD151 in promoting cell adhesion, migration, and metastasis (Kohno et al., 2002; Palmer et al., 2014; Shigeta et al., 2003; Zijlstra et al., 2008). Several studies have shown an emerging role for CD151 in cell proliferation under specific contexts. CD151 can modulate tumor growth downstream of hepatocyte growth factor (HGF) (Franco et al., 2010); depletion of CD151 can impair TGF-β-induced proliferation and metastasis (Sadej et al., 2010); breast cancer cells grown on laminin-5 acquire ECM (extracellular-matrix)-mediated resistance to anti-HER2 agents, such as trastuzumab and lapatinib; and depletion of CD151 can revert this resistant phenotype (Yang et al., 2010). We report a previously unidentified role for CD151 in directly promoting the survival of cancer cells. Our observation that CD151 dependency varies across HGSC cell lines is indicative of the inherent complexity within this tumor type and the myriad possible biological functions of CD151 in human cancers.

Our findings that CD151 dependency coincides with high expression of ZEB1 and ZEB2 and that each are necessary for mediating sensitivity to CD151 suppression emphasize the importance of CD151 in cells that exhibit mesenchymal features. CD151 cooperates with integrin α_6 to promote EMT in hepatocellular carcinoma cells (Ke et al., 2011); miR-506 can target *VIM*, *SNAI2*, and *CD151* and regulate EMT in breast cancer and HGSC (Arora et al., 2013; Yang et al., 2013); and CD151 is a marker of chondrogenic differentiation in human mesenchymal stem cells (Lee et al., 2009). CD151 has a multitude of known interacting partners, in particular, integrins $\alpha_3\beta_1$, $\alpha_6\beta_1$, $\alpha_6\beta_4$, $\alpha_7\beta_1$, EGFR, c-MET, PI4KII, and PKCα, which may contribute to the spatial organization of CD151. Integrin-free CD151 occurs at a higher proportion in CD151-dependent versus CD151-independent cell lines, suggesting that CD151 complexes can vary between different cell states. Whether the requirement for CD151 in cell survival is mediated by its function in distinct complexes remains to be elucidated.

Comparison of the CD151-dependency and HGSC-subtype gene signatures indicates that CD151-dependent cells share features of the mesenchymal subtype, which has the worst outcome (Verhaak et al., 2013). Currently, there are no therapies in clinic targeting a specific subtype or reports of subtype-specific therapies. Targeting CD151 may represent an intervention opportunity in the mesenchymal subgroup of HGSC, and the CD151-dependency signature (namely, ZEB1^{hi}/ZEB2^{hi}/E-cadherin^{lo}) might serve as a biomarker to identify patients with responsive tumors. High CD151 expression was strongly associated with poor outcome to a similar degree as that of the TCGA prognostic gene signature (Verhaak et al., 2013). CD151 expression may be a relevant marker for predicting outcome in HGSC comparable to current models, and therefore, head-to-head comparisons are needed.

The observations that CD151 has both pro-survival and pro-migratory functions make it an attractive therapeutic target. Clinically, targeting CD151 directly could affect cell survival, and anti-CD151 mAbs, which have been reported to affect metastasis in vivo (Palmer et al., 2014; Zijlstra et al., 2008), may have utility in preventing tumor cell dissemination and peritoneal spread, the major cause of lethality in HGSC. We found that CD151-independent cell lines were more susceptible to small molecules targeting EGFR, consistent with previous reports suggesting an inverse association between EGFR inhibitor response and an EMT phenotype (Byers et al., 2013; Shien et al., 2013). Based on our observations, we would predict that screening HGSC tumors with low ZEB1/ZEB2 expression and high E-cadherin expression, as well as other features of CD151-independent cells, might enrich for patient populations most likely to respond to EGFR antagonists. Furthermore, targeting tumors with a combination of EGFR antagonists and CD151-directed therapies might achieve improved clinical response.

The role of CD151 in HGSC may extend beyond its pro-survival effects. CD151 is the major interaction partner of laminin-binding integrins, and the laminin subunit LAMC1 is exclusively overexpressed in STIC lesions, precursor lesions of HGSCs (Kuhn et al., 2012). Laminin is required for promoting a cancer stem cell phenotype in other malignancies, such as glioblastoma multiforme (Pollard et al., 2009). We propose that a laminin-CD151 axis may be important in the early development of HGSC and in the maintenance of a cancer stem-like population.

In summary, integration of functional genomics and interrogation of genes encoding cell-surface molecules in HGSC cells revealed dependency on CD151. Targeting CD151 has the potential to impair HGSC tumor growth and tumor cell dissemination, and future work will be aimed at developing CD151-directed therapeutics to address the utility of CD151 as a therapeutic

Figure 5. CD151 Dependency Is Coupled to a ZEB1 and ZEB2 Transcription Factor Network

(A) Top differentially expressed genes positively and negatively correlated with CD151 dependency. Mesenchymal and epithelial differentiation-related genes are indicated in red and blue, respectively.

(B) Immunoblot analysis of selected differentially expressed proteins between CD151-dependent (red) and CD151-independent (blue) cells. CD151 dependency was not examined in the remaining cell lines. Actin serves as a protein loading control.

(C) Enrichment plot for the COLDREN_GEFITINIB_RESISTANCE_DN gene set from gene set enrichment analysis (GSEA) of CD151-independent cell lines. The full list is available in Table S2. NES, normalized enrichment score.

(D) Small molecules with toxicity profiles significantly correlated with CD151 dependency. Compounds annotated to target epidermal growth factor receptor (EGFR) are shown in red.

(E and F) Relative viability of CD151-dependent (red) and -independent (blue) cells exposed to (E) erlotinib and (F) gefitinib for 72 hr. Error bars indicate mean ± SEM; n = 3. GI_{50} (50% of maximal inhibition of cell proliferation) values greater than the highest tested dose (30 μM) were reported as 30 μM.

See also Figure S5, Table S2, and Data File S2.

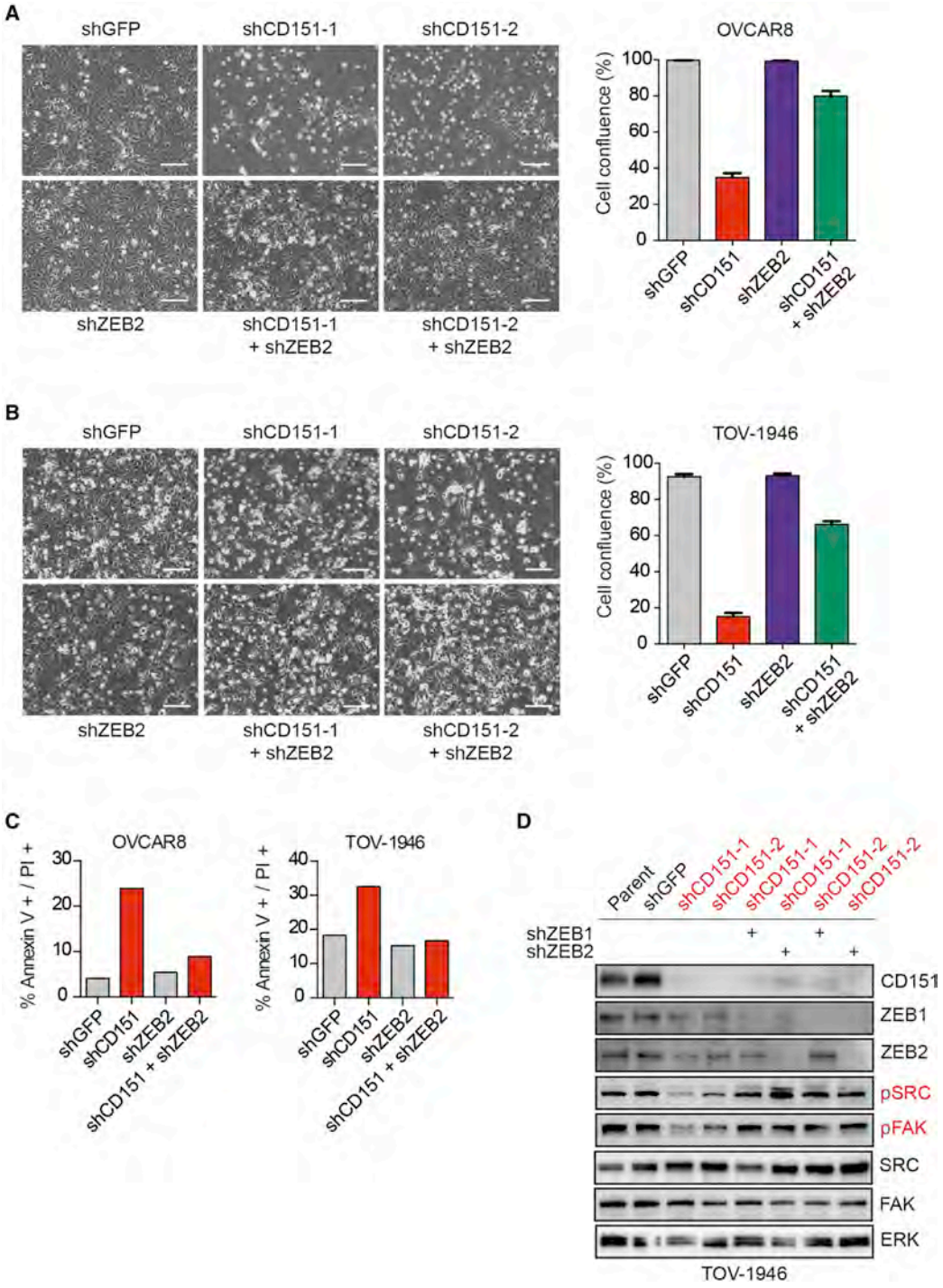

Figure 6. ZEB1 and ZEB2 Mediate Sensitivity to CD151 Suppression

(A and B) Phase-contrast images (left) and cell confluence quantification (right) of (A) OVCAR8 and (B) TOV-1946 cells expressing shGFP and hairpins targeting CD151 and/or ZEB2. Scale bars represent 100 μm. Error bars indicate mean ± SEM; n = 4.

(C) Flow cytometry analysis of annexin V and propidium iodide (PI) staining in OVCAR8 and TOV-1946 cells expressing shGFP or shRNA targeting CD151 and/or ZEB2. Percentages of annexin-V- and PI-positive cells are shown.

(D) Immunoblot analysis of phosphorylated SRC (pSRC) and phosphorylated FAK (pFAK) in TOV-1946 cells expressing control shGFP or shRNA targeting CD151 and/or ZEB1 and ZEB2. ERK serves as a protein loading control.

See also Figure S6.

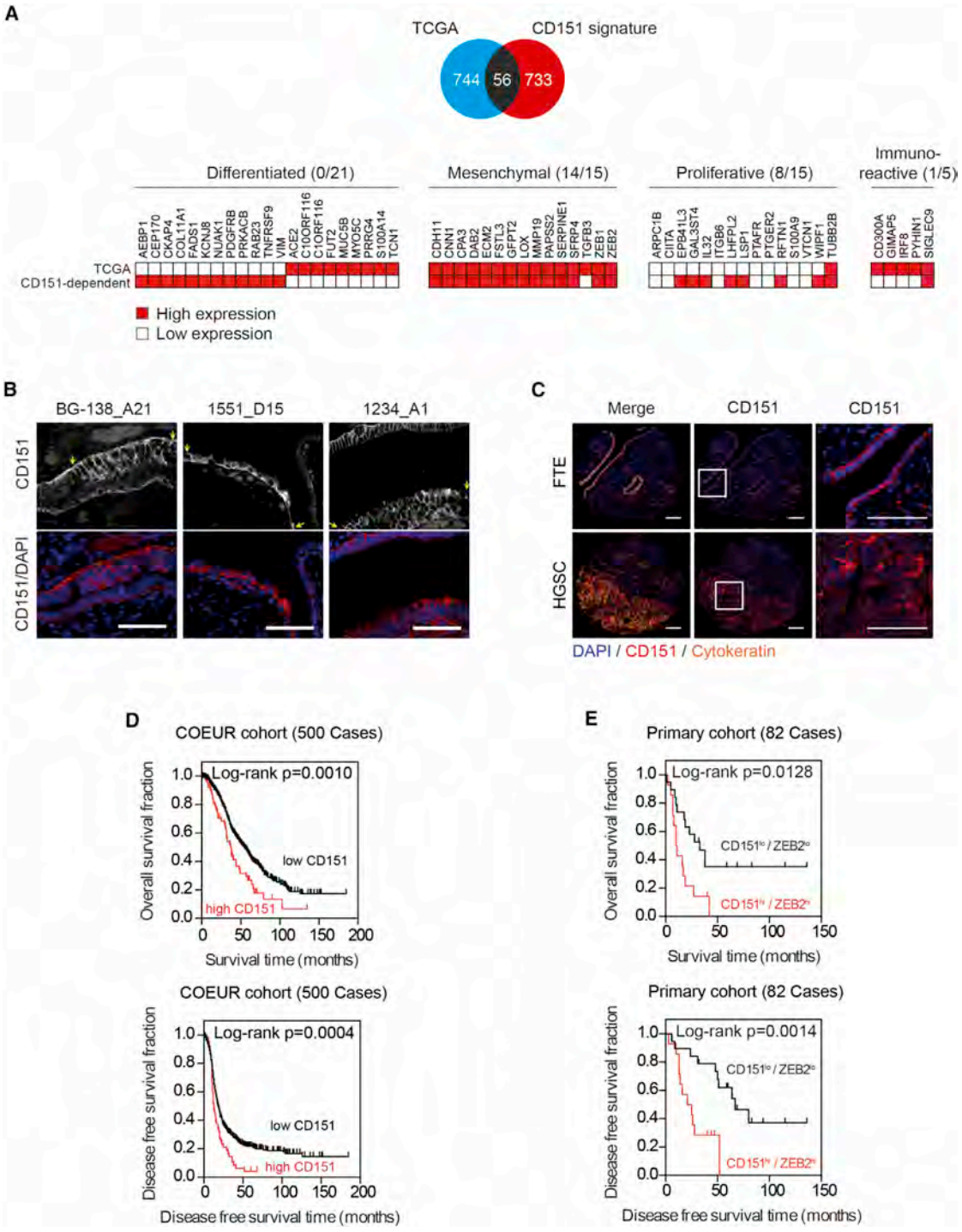

Figure 7. The CD151-Dependent Phenotype Resembles the Mesenchymal Subtype of HGSC and High CD151 Expression Is Associated with Poor Prognosis

(A) Overlap of TCGA subtype signature genes and CD151-dependency-associated genes. Genes denoted in red were upregulated in the specified TCGA subtype and in CD151-dependent cells; genes denoted in white were downregulated. Indicated is the number of genes concordant between the TCGA subtype and CD151-dependent cells.

(B) Representative immunofluorescence staining of CD151 alone (top) and merged with DAPI (bottom) in STIC precursor lesions from three independent patient samples. Arrows mark the boundaries of the STIC lesion. Scale bars represent 100 μm.

(legend continued on next page)

target. Our findings highlight the importance of developing targeted approaches for treating HGSC and present a possible strategy for ultimately improving the prognosis of women with this devastating disease.

EXPERIMENTAL PROCEDURES

Detailed information is provided in the Supplemental Experimental Procedures.

Animal Studies

All animal studies were carried out using protocols that have been approved by the University Health Network Animal Care Committee. See the Supplemental Experimental Procedures.

Cell-Surface Marker Profiling

Cell-surface antibody screens were performed as previously described (Gedye et al., 2014). See the Supplemental Experimental Procedures.

Kinase Inhibitor Screen

Cells were plated at a density of 0.3–1 × 10^4 cells per well in 96-well plates and were incubated overnight to allow cells to adhere. A library of 400 kinase inhibitors (provided by the Ontario Institute for Cancer Research) or DMSO was added by a Robot Pin Tool System to a final concentration of 2 μM for 72 hr. Viability was determined using alamarBlue (Invitrogen) according to the manufacturer's protocol, and fluorescence was quantified using a PHERAstar detection system. Values were median normalized across all compounds and visualized using R. Correlation of relative viability with CD151 dependency was performed using Pearson correlation. Inhibitors with relative viability values greater than 0.7 across all lines were not included in the correlation analysis.

EtBr Incorporation Assay

Cell lines were seeded in low-adhesion 96-well round bottom plates (Corning) at a density of 75–150 cells per well. Cells were spun at 900 rpm for 3 min to form cellular clusters. To follow EtBr incorporation in live clusters, 2 μM EtBr (Molecular Probes) was included in the media during cell seeding. Phase-contrast and fluorescent images of cellular clusters were acquired every 20–30 min, and the level of EtBr incorporation was quantified by measuring changes in the total number of pixels (red channel) present within cellular clusters over time. The quantification of EtBr incorporation was performed using Nikon NIS Elements AR software. See the Supplemental Experimental Procedures.

Mesothelial Clearance Assay

Mesothelial cells were plated on glass-bottomed dishes (Mat-TEK) coated with 5 μg/mL fibronectin (Sigma). Cells were maintained in culture until confluent (48 hr after plating). To generate cell clusters, OVCAR8 or PEA1 cells were dissociated by trypsinization, washed twice with PBS, resuspended in media, and plated in low-adhesion culture dishes (Corning). Cell clusters were collected for experiments 12–16 hr later. In co-culture experiments, cell clusters were added to a confluent mesothelial monolayer expressing GFP, allowed to attach for 30–60 min, and imaged for 8 hr using a Nikon Ti-E Inverted Motorized Widefield Fluorescence Microscope. Cellular clusters that remained attached during the experiment were used for quantification. Mesothelial clearance was quantified as previously described (Iwanicki et al., 2011).

shRNA Screens

Lentiviral hairpin dropout screens were performed as previously described (Marcotte et al., 2012). See Supplemental Experimental Procedures.

Statistical Analyses

Values are expressed as means ± SEM. Experiments were performed three times, and two-sided t tests were performed to determine statistical significance between samples, unless otherwise indicated. Means with $p < 0.05$ were considered statistically significant.

ACCESSION NUMBERS

The accession number for the RNA-seq analysis reported in this paper is GEO: GSE94304.

SUPPLEMENTAL INFORMATION

Supplemental Information includes Supplemental Experimental Procedures, seven figures, three tables, two movies, and two data files and can be found with this article online at http://dx.doi.org/10.1016/j.celrep.2017.02.028.

AUTHOR CONTRIBUTIONS

Conceptualization, M.M. and R.R.; Methodology, M.M., L.C., K.R.B., M.I., J.P., J.N., F.S., P.K., S.A.D., F.S.S., and M.N.; Investigation, M.M., L.C., K.R.B., M.I., J.P., J.N., F.S., P.K., S.A.D., and M.N.; Data Curation Management, M.M., K.R.B., F.S., P.K., and F.S.S.; Writing – Original Draft, M.M. and R.R.; Writing – Review & Editing, M.M., J.C., and R.R.; Funding Acquisition, M.M. and R.R.; Resources, B.G.N., J.M., R.D., R.A., L.A., A.-M.M.-M., and R.R.; Supervision, B.G.N., L.A., A.-M.M.-M., and R.R.

ACKNOWLEDGMENTS

We thank J. Brenton (Cancer Research UK), P. Tonin (McGill University), and G. Fletcher (UHN) for sharing cell lines; Andries Zijlstra for providing mAb 1A5; OICR Medicinal Chemistry and Lunenfeld-Tanenbaum Robotics and High Throughput Screening Facility for assistance with kinase inhibitor screening; the UHN animal facility for assistance with animal studies; and the UHN Microarray Centre for assistance with RNA-seq and copy number analysis. This study used resources provided by the Canadian Ovarian Cancer Research Consortium's biobank funded by the Terry Fox Research Institute (grant no. 2012-46). The Consortium acknowledges contributions to the biobank from institutions across Canada (http://www.tfri.ca/COEUR/members). This work was supported by Ovarian Cancer Canada's Teal Heart Scholarship Fund (M.M.), the Fond de Recherche en Santé du Québec (FRSQ) grant 33657 (L.C.), and funding by the OICR, grants STP and ITV (R.R.).

Received: May 5, 2016
Revised: December 20, 2016
Accepted: February 8, 2017
Published: March 7, 2017

REFERENCES

Abeysinghe, H.R., Cao, Q., Xu, J., Pollock, S., Veyberman, Y., Guckert, N.L., Keng, P., and Wang, N. (2003). THY1 expression is associated with tumor suppression of human ovarian cancer. Cancer Genet. Cytogenet. *143*, 125–132.

(C) Representative immunofluorescence staining of CD151 (red) in normal fallopian tube epithelium (FTE, top) and HGSC tumor (bottom). Epithelial cells were identified by cytokeratin (keratin7/18/19$^+$, yellow) and nuclei by DAPI staining. The highlighted region in the middle column is shown at a higher magnification in the right column. Scale bars represent 100 μm.
(D) Kaplan-Meier plots for overall survival and disease-free survival of 500 HGSC patients dichotomized into CD151-high (n = 72)- and CD151-low (n = 428)-expressing tumors.
(E) Kaplan-Meier plots for overall survival and disease-free survival from a primary cohort of 82 patients classified as CD151^{lo}ZEB2^{lo} (n = 19)- and CD151^{hi}ZEB2^{hi} (n = 14)-expressing tumors.
See also Figure S7 and Table S3.

Aigner, K., Dampier, B., Descovich, L., Mikula, M., Sultan, A., Schreiber, M., Mikulits, W., Brabletz, T., Strand, D., Obrist, P., et al. (2007). The transcription factor ZEB1 (deltaEF1) promotes tumour cell dedifferentiation by repressing master regulators of epithelial polarity. Oncogene *26*, 6979–6988.

Arima, Y., Hayashi, H., Sasaki, M., Hosonaga, M., Goto, T.M., Chiyoda, T., Kuninaka, S., Shibata, T., Ohata, H., Nakagama, H., et al. (2012). Induction of ZEB proteins by inactivation of RB protein is key determinant of mesenchymal phenotype of breast cancer. J. Biol. Chem. *287*, 7896–7906.

Arora, H., Qureshi, R., and Park, W.Y. (2013). miR-506 regulates epithelial mesenchymal transition in breast cancer cell lines. PLoS ONE *8*, e64273.

Baldwin, L.A., Hoff, J.T., Lefringhouse, J., Zhang, M., Jia, C., Liu, Z., Erfani, S., Jin, H., Xu, M., She, Q.B., et al. (2014). CD151-α3β1 integrin complexes suppress ovarian tumor growth by repressing slug-mediated EMT and canonical Wnt signaling. Oncotarget *5*, 12203–12217.

Barbie, D.A., Tamayo, P., Boehm, J.S., Kim, S.Y., Moody, S.E., Dunn, I.F., Schinzel, A.C., Sandy, P., Meylan, E., Scholl, C., et al. (2009). Systematic RNA interference reveals that oncogenic KRAS-driven cancers require TBK1. Nature *462*, 108–112.

Bast, R.C., Jr., Hennessy, B., and Mills, G.B. (2009). The biology of ovarian cancer: new opportunities for translation. Nat. Rev. Cancer *9*, 415–428.

Brabletz, S., and Brabletz, T. (2010). The ZEB/miR-200 feedback loop–a motor of cellular plasticity in development and cancer? EMBO Rep. *11*, 670–677.

Burger, R.A., Brady, M.F., Bookman, M.A., Fleming, G.F., Monk, B.J., Huang, H., Mannel, R.S., Homesley, H.D., Fowler, J., Greer, B.E., et al.; Gynecologic Oncology Group (2011). Incorporation of bevacizumab in the primary treatment of ovarian cancer. N. Engl. J. Med. *365*, 2473–2483.

Burleson, K.M., Casey, R.C., Skubitz, K.M., Pambuccian, S.E., Oegema, T.R., Jr., and Skubitz, A.P. (2004). Ovarian carcinoma ascites spheroids adhere to extracellular matrix components and mesothelial cell monolayers. Gynecol. Oncol. *93*, 170–181.

Byers, L.A., Diao, L., Wang, J., Saintigny, P., Girard, L., Peyton, M., Shen, L., Fan, Y., Giri, U., Tumula, P.K., et al. (2013). An epithelial-mesenchymal transition gene signature predicts resistance to EGFR and PI3K inhibitors and identifies Axl as a therapeutic target for overcoming EGFR inhibitor resistance. Clin. Cancer Res. *19*, 279–290.

Cancer Genome Atlas Research Network (2011). Integrated genomic analyses of ovarian carcinoma. Nature *474*, 609–615.

Desgrosellier, J.S., and Cheresh, D.A. (2010). Integrins in cancer: biological implications and therapeutic opportunities. Nat. Rev. Cancer *10*, 9–22.

Domcke, S., Sinha, R., Levine, D.A., Sander, C., and Schultz, N. (2013). Evaluating cell lines as tumour models by comparison of genomic profiles. Nat. Commun. *4*, 2126.

Ferlay, J., Soerjomataram, I., Dikshit, R., Eser, S., Mathers, C., Rebelo, M., Parkin, D.M., Forman, D., and Bray, F. (2015). Cancer incidence and mortality worldwide: sources, methods and major patterns in GLOBOCAN 2012. Int. J. Cancer *136*, E359–E386.

Franco, M., Muratori, C., Corso, S., Tenaglia, E., Bertotti, A., Capparuccia, L., Trusolino, L., Comoglio, P.M., and Tamagnone, L. (2010). The tetraspanin CD151 is required for Met-dependent signaling and tumor cell growth. J. Biol. Chem. *285*, 38756–38764.

Gedye, C.A., Hussain, A., Paterson, J., Smrke, A., Saini, H., Sirskyj, D., Pereira, K., Lobo, N., Stewart, J., Go, C., et al. (2014). Cell surface profiling using high-throughput flow cytometry: a platform for biomarker discovery and analysis of cellular heterogeneity. PLoS ONE *9*, e105602.

Gerber, H.P., Koehn, F.E., and Abraham, R.T. (2013). The antibody-drug conjugate: an enabling modality for natural product-based cancer therapeutics. Nat. Prod. Rep. *30*, 625–639.

Haeuw, J.F., Goetsch, L., Bailly, C., and Corvaia, N. (2011). Tetraspanin CD151 as a target for antibody-based cancer immunotherapy. Biochem. Soc. Trans. *39*, 553–558.

Hart, T., Chandrashekhar, M., Aregger, M., Steinhart, Z., Brown, K.R., MacLeod, G., Mis, M., Zimmermann, M., Fradet-Turcotte, A., Sun, S., et al. (2015). High-resolution CRISPR screens reveal fitness genes and genotype-specific cancer liabilities. Cell *163*, 1515–1526.

Hemler, M.E. (2005). Tetraspanin functions and associated microdomains. Nat. Rev. Mol. Cell Biol. *6*, 801–811.

Hover, L.D., Young, C.D., Bhola, N.E., Wilson, A.J., Khabele, D., Hong, C.C., Moses, H.L., and Owens, P. (2015). Small molecule inhibitor of the bone morphogenetic protein pathway DMH1 reduces ovarian cancer cell growth. Cancer Lett. *368*, 79–87.

Iwanicki, M.P., Davidowitz, R.A., Ng, M.R., Besser, A., Muranen, T., Merritt, M., Danuser, G., Ince, T.A., and Brugge, J.S. (2011). Ovarian cancer spheroids use myosin-generated force to clear the mesothelium. Cancer Discov. *1*, 144–157.

Kajiyama, H., Kikkawa, F., Khin, E., Shibata, K., Ino, K., and Mizutani, S. (2003). Dipeptidyl peptidase IV overexpression induces up-regulation of E-cadherin and tissue inhibitors of matrix metalloproteinases, resulting in decreased invasive potential in ovarian carcinoma cells. Cancer Res. *63*, 2278–2283.

Ke, A.W., Shi, G.M., Zhou, J., Huang, X.Y., Shi, Y.H., Ding, Z.B., Wang, X.Y., Devbhandari, R.P., and Fan, J. (2011). CD151 amplifies signaling by integrin alpha6beta1 to PI3K and induces the epithelial-mesenchymal transition in HCC cells. Gastroenterology *140*, 1629–1641.e1615.

Kim, H.S., Mendiratta, S., Kim, J., Pecot, C.V., Larsen, J.E., Zubovych, I., Seo, B.Y., Kim, J., Eskiocak, B., Chung, H., et al. (2013). Systematic identification of molecular subtype-selective vulnerabilities in non-small-cell lung cancer. Cell *155*, 552–566.

Kohn, K.W., Zeeberg, B.M., Reinhold, W.C., and Pommier, Y. (2014). Gene expression correlations in human cancer cell lines define molecular interaction networks for epithelial phenotype. PLoS ONE *9*, e99269.

Kohno, M., Hasegawa, H., Miyake, M., Yamamoto, T., and Fujita, S. (2002). CD151 enhances cell motility and metastasis of cancer cells in the presence of focal adhesion kinase. Int. J. Cancer *97*, 336–343.

Kuhn, E., Kurman, R.J., Soslow, R.A., Han, G., Sehdev, A.S., Morin, P.J., Wang, T.L., and Shih, IeM. (2012). The diagnostic and biological implications of laminin expression in serous tubal intraepithelial carcinoma. Am. J. Surg. Pathol. *36*, 1826–1834.

Kumar, S.R., Masood, R., Spannuth, W.A., Singh, J., Scehnet, J., Kleiber, G., Jennings, N., Deavers, M., Krasnoperov, V., Dubeau, L., et al. (2007). The receptor tyrosine kinase EphB4 is overexpressed in ovarian cancer, provides survival signals and predicts poor outcome. Br. J. Cancer *96*, 1083–1091.

Lee, H.J., Choi, B.H., Min, B.H., and Park, S.R. (2009). Changes in surface markers of human mesenchymal stem cells during the chondrogenic differentiation and dedifferentiation processes in vitro. Arthritis Rheum. *60*, 2325–2332.

Liu, F.S., Dong, J.T., Chen, J.T., Hsieh, Y.T., Ho, E.S., and Hung, M.J. (2000). Frequent down-regulation and lack of mutation of the KAI1 metastasis suppressor gene in epithelial ovarian carcinoma. Gynecol. Oncol. *78*, 10–15.

Luo, B., Cheung, H.W., Subramanian, A., Sharifnia, T., Okamoto, M., Yang, X., Hinkle, G., Boehm, J.S., Beroukhim, R., Weir, B.A., et al. (2008). Highly parallel identification of essential genes in cancer cells. Proc. Natl. Acad. Sci. USA *105*, 20380–20385.

Marcotte, R., Brown, K.R., Suarez, F., Sayad, A., Karamboulas, K., Krzyzanowski, P.M., Sircoulomb, F., Medrano, M., Fedyshyn, Y., Koh, J.L., et al. (2012). Essential gene profiles in breast, pancreatic, and ovarian cancer cells. Cancer Discov. *2*, 172–189.

Marcotte, R., Sayad, A., Brown, K.R., Sanchez-Garcia, F., Reimand, J., Haider, M., Virtanen, C., Bradner, J.E., Bader, G.D., Mills, G.B., et al. (2016). Functional genomic landscape of human breast cancer drivers, vulnerabilities, and resistance. Cell *164*, 293–309.

Moffat, J., Grueneberg, D.A., Yang, X., Kim, S.Y., Kloepfer, A.M., Hinkle, G., Piqani, B., Eisenhaure, T.M., Luo, B., Grenier, J.K., et al. (2006). A lentiviral RNAi library for human and mouse genes applied to an arrayed viral high-content screen. Cell *124*, 1283–1298.

Palmer, T.D., Martínez, C.H., Vasquez, C., Hebron, K.E., Jones-Paris, C., Arnold, S.A., Chan, S.M., Chalasani, V., Gomez-Lemus, J.A., Williams, A.K., et al. (2014). Integrin-free tetraspanin CD151 can inhibit tumor cell motility

upon clustering and is a clinical indicator of prostate cancer progression. Cancer Res. *74*, 173–187.

Pollard, S.M., Yoshikawa, K., Clarke, I.D., Danovi, D., Stricker, S., Russell, R., Bayani, J., Head, R., Lee, M., Bernstein, M., et al. (2009). Glioma stem cell lines expanded in adherent culture have tumor-specific phenotypes and are suitable for chemical and genetic screens. Cell Stem Cell *4*, 568–580.

Ratner, E.S., Sartorelli, A.C., and Lin, Z.P. (2012). Poly (ADP-ribose) polymerase inhibitors: on the horizon of tailored and personalized therapies for epithelial ovarian cancer. Curr. Opin. Oncol. *24*, 564–571.

Sadej, R., Romanska, H., Kavanagh, D., Baldwin, G., Takahashi, T., Kalia, N., and Berditchevski, F. (2010). Tetraspanin CD151 regulates transforming growth factor beta signaling: implication in tumor metastasis. Cancer Res. *70*, 6059–6070.

Sheng, Q., Liu, X., Fleming, E., Yuan, K., Piao, H., Chen, J., Moustafa, Z., Thomas, R.K., Greulich, H., Schinzel, A., et al. (2010). An activated ErbB3/NRG1 autocrine loop supports in vivo proliferation in ovarian cancer cells. Cancer Cell *17*, 298–310.

Shien, K., Toyooka, S., Yamamoto, H., Soh, J., Jida, M., Thu, K.L., Hashida, S., Maki, Y., Ichihara, E., Asano, H., et al. (2013). Acquired resistance to EGFR inhibitors is associated with a manifestation of stem cell-like properties in cancer cells. Cancer Res. *73*, 3051–3061.

Shigeta, M., Sanzen, N., Ozawa, M., Gu, J., Hasegawa, H., and Sekiguchi, K. (2003). CD151 regulates epithelial cell-cell adhesion through PKC- and Cdc42-dependent actin cytoskeletal reorganization. J. Cell Biol. *163*, 165–176.

Song, Y., Washington, M.K., and Crawford, H.C. (2010). Loss of FOXA1/2 is essential for the epithelial-to-mesenchymal transition in pancreatic cancer. Cancer Res. *70*, 2115–2125.

Tothill, R.W., Tinker, A.V., George, J., Brown, R., Fox, S.B., Lade, S., Johnson, D.S., Trivett, M.K., Etemadmoghadam, D., Locandro, B., et al.; Australian Ovarian Cancer Study Group (2008). Novel molecular subtypes of serous and endometrioid ovarian cancer linked to clinical outcome. Clin. Cancer Res. *14*, 5198–5208.

Verhaak, R.G., Tamayo, P., Yang, J.Y., Hubbard, D., Zhang, H., Creighton, C.J., Fereday, S., Lawrence, M., Carter, S.L., Mermel, C.H., et al.; Cancer Genome Atlas Research Network (2013). Prognostically relevant gene signatures of high-grade serous ovarian carcinoma. J. Clin. Invest. *123*, 517–525.

Weinstein, I.B. (2002). Cancer. Addiction to oncogenes–the Achilles heal of cancer. Science *297*, 63–64.

Yang, X.H., Flores, L.M., Li, Q., Zhou, P., Xu, F., Krop, I.E., and Hemler, M.E. (2010). Disruption of laminin-integrin-CD151-focal adhesion kinase axis sensitizes breast cancer cells to ErbB2 antagonists. Cancer Res. *70*, 2256–2263.

Yang, D., Sun, Y., Hu, L., Zheng, H., Ji, P., Pecot, C.V., Zhao, Y., Reynolds, S., Cheng, H., Rupaimoole, R., et al. (2013). Integrated analyses identify a master microRNA regulatory network for the mesenchymal subtype in serous ovarian cancer. Cancer Cell *23*, 186–199.

Yang, T., Li, X.N., Li, X.G., Li, M., and Gao, P.Z. (2014). DNAJC6 promotes hepatocellular carcinoma progression through induction of epithelial-mesenchymal transition. Biochem. Biophys. Res. Commun. *455*, 298–304.

Zavadil, J., and Böttinger, E.P. (2005). TGF-beta and epithelial-to-mesenchymal transitions. Oncogene *24*, 5764–5774.

Zhou, S.L., Zhou, Z.J., Hu, Z.Q., Li, X., Huang, X.W., Wang, Z., Fan, J., Dai, Z., and Zhou, J. (2015). CXCR2/CXCL5 axis contributes to epithelial-mesenchymal transition of HCC cells through activating PI3K/Akt/GSK-3β/Snail signaling. Cancer Lett. *358*, 124–135.

Zijlstra, A., Lewis, J., Degryse, B., Stuhlmann, H., and Quigley, J.P. (2008). The inhibition of tumor cell intravasation and subsequent metastasis via regulation of in vivo tumor cell motility by the tetraspanin CD151. Cancer Cell *13*, 221–234.